Catalysis Today 152 (2010) 54–60

Contents lists available at ScienceDirect

Catalysis Today

journal homepage: www.elsevier.com/locate/cattod

Improved large mesoporous ordered molecular sieves—Stabilization and acid/base functionalization

Hendrik Kosslick[a,*], Irene Pitsch[a], Jens Deutsch[a], Marga-Martina Pohl[a], Axel Schulz[a,b], Vu Anh Tuan[c], Nguyen Dinh Tuyen[c], Ligia Frunza[d], Christian Jaeger[e]

[a] Leibniz Institute for Catalysis e.V. at the University of Rostock Albert-Einstein-Str. 29a, D-18059 Rostock, Germany
[b] Institute of Chemistry, University of Rostock, Albert-Einstein-Str. 3a, D-18059 Rostock, Germany
[c] Institute of Chemistry, Vietnam Academy of Science and Technology (VAST), 18 Hoang Quoc Viet, Cau Giay, Hanoi, Viet Nam
[d] National Institute of Material Physics, Atomistilor Str. 105, R-077125 Magurele, Romania
[e] BAM – Federal Institute for Materials Research and Testing, Division I.3, Working Group NMR Spectroscopy, Richard-Willstätter Str. 11, D-12489 Berlin, Germany

ARTICLE INFO

Keywords:
Nanoporous molecular sieve
Al substitution
Stability
Synthesis
Acidity
Catalysis

ABSTRACT

The preparation of nanoporous materials with enhanced stability using an improved synthesis route using reactive inorganic silica and alumina species is reported. This way improved mesoporous molecular sieves were obtained. The synthesized aluminum substituted mesoporous molecular materials (Al-MMS) contain very large pores of 50–200 Å size combined with an improved pore wall thickness. Increased wall thickness and Al substitution lead to an improved chemical stability against alkaline solution. The textural, structural and acid properties are investigated by physico-chemical methods. The catalytic performance acidic materials was tested in the benzoylation reaction; amino functionalized materials were studied in the base catalyzed Michael addition.

1. Introduction

Ordered mesoporous materials attract growing attention because of their wide potential of application in catalysis, separation, biotechnology, etc. [1–7]. The accessibility of acid/basic sites, the diffusivity of larger molecules or the immobilization of catalytic complexes and enzymes are crucial for the desired application. Despite of the achieved progress, the preparation of large porous ordered aluminosilicates is still challenge. The pore structure of ordered mesoporous materials like SBA-15 is rather complex [8]. Synthesis conditions strongly influence the textural properties as pore size, shape and pore volume, pore connectivity and particle morphology [9–11]. Hard-templating allows the formation of nano-macroporous materials [12]. Pore design influences the catalytic properties by access to active sites [13]. Also hydrothermal stability [14] may enhanced by presence of some micropores in the pore walls [15]. The incorporation of aluminum into the silicate network is of special importance for creation of acid sites. Beside direct hydrothermal synthesis of aluminium substituted mesoporous materials [9,10] post-synthesis modification by treatment of pure siliceous mesoporous materials with aluminium chloride and other aluminium sources has been investigated [16–19]. Lewis and Brønsted acidic materials have been obtained [9,12,19]. In some cases formation of strong Lewis acid sites [20] or pure Brønsted acidic materials [21,22] has been emphasized. The Si/Al ratio of mesoporous molecular sieves could be extended down to 7 and or 5.5, respectively [9,19]. Silylation of surface silanol groups allow functionalization of mesoporous molecular sieves with sulfonic acid and base amino groups [23,24].

In this contribution the preparation of nanoporous materials with enhanced stability will be reported. An improved synthesis route using reactive inorganic silica and alumina species is presented. This way synthesized Al-MMS materials contain very large pores of 50–200 Å size combined with an improved pore wall thickness. Increased wall thickness and Al substitution lead to an improved chemical stability against alkaline solution. The textural, structural and acid properties are investigated by physico-chemical methods. The catalytic performance of amino functionalized materials has been studied in the base catalyzed Michael addition. The results show, that the large pore sizes combined with interconnectivity of the pores allow the formation of large molecules.

2. Experimental

2.1. Synthesis

Ordered aluminum substituted silicates (Al-MMS) were prepared by hydrothermal treatment starting with template con-

* Corresponding author. Tel.: +49 381 4986384; fax: +49 381 4986382.
E-mail address: Hendrik.Kosslick@catalysis.de (H. Kosslick).

0920-5861/$ – see front matter © 2010 Elsevier B.V. All rights reserved.
doi:10.1016/j.cattod.2010.03.005

taining reaction gels. The composition and treatment of prepared reaction mixtures were similar to SBA-15 synthesis [25]. Pluronic P123 was used as template. Mesitylene acted as pore size enlarging spacer. Chemicals were of p.a. grade and purchased from Aldrich and Fluka, respectively. In contrast to usual SBA-15 synthesis procedures, a reactive inorganic silica precursor and Al-oxo-hydroxo species were used as alumina source. The reactive silica was prepared by ion exchange of water glass over an acidified organic resin. The obtained fresh silica solution was immediately mixed with the alumina source. The Si/Al ratio of the synthesis gel was varied between 1 and 25. Thereafter, the template was added under vigorous stirring. The obtained reaction gels were hydrothermal treated at elevate temperature for 2–4 days under autogeneous pressure. The recovered reaction product was washed, dried and calcined at 550 °C. Exchange of residual sodium ions by ammonium was carried out by stirring the calcined Al-MMS material in diluted ammonium nitrate solution at 60 °C.

2.2. Functionalization

For acid functionalization of MMS materials 1 g of calcined and pre-dried samples were treated with 3.5 mmol of triethoxy(mercaptopropyl) silane in toluene under reflux for 2 h. The obtained mercaptosilylated material was oxidized to sulfonic acid using hydrogen peroxide.

For grafting of basic function, calcined Al-MMS samples were stirred with aminopropyl- and N-dimethylaminopropyl silane of different basicity in toluene under reflux.

2.3. Characterization

Samples were characterized by TEM, XRD, nitrogen sorption, ammonia TPD and pyridine FTIR and ^{13}C, ^{27}Al and ^{29}Si MAS solid state NMR spectrometry as reported elsewhere [26,27]. The chemical compositions of mesoporous materials were determined by CHNS and ICP AES analysis.

2.4. Catalysis

Catalytic testing of acid and base functionalized mesoporous molecular sieves was performed in the liquid phase in organic solvents under batch conditions using glassy reaction vessels under stirring. The catalytic performance of acidic materials was tested in the benzoylation reaction. Reaction conditions: 12 ml anisol, 0.6 g benzoic anhydride, 200 mg catalyst, reaction time; 3 h, temperature: 50 °C. 0.1 g benzoic acid-n-butylester was added as internal standard for HPLC-analysis. The Michael addition reaction of methyl-vinyl-ketone and 2-methyl-cyclohexane-1,3-dione was used for catalytic testing of base functionalized of MMS materials.

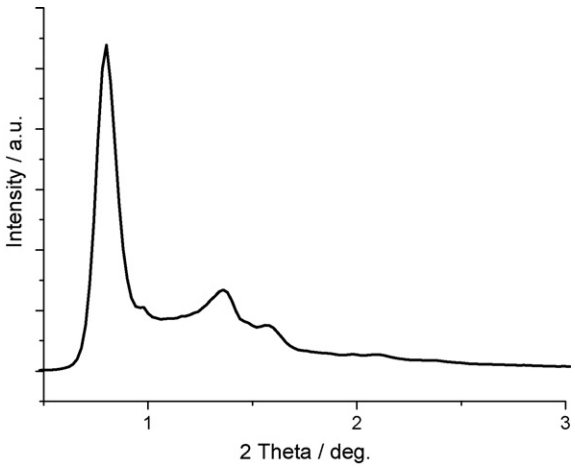

Fig. 1. X-ray diffraction pattern of calcined Al-MMS.

3. Results and discussion

3.1. Synthesis

The new synthesis approach, using reactive inorganic silica and alumina precursors as starting materials and Pluronic P123 as template yields highly ordered mesoporous aluminosilicate materials as indicated by the XRD pattern (Fig. 1). By using mesitylene as additive the pore size could be extended up to 200 Å. This extra large porous material shows, however, a foam-like structure. The well ordering of the pore structure is also confirmed by the TEM images (Fig. 2). They show ordered parallel arranged interconnected pores of uniform size (50–100 Å). Interestingly, the Al-MMS materials have increased thickness of pore walls of 40–50 Å. This is a prerequisite for an improved stability of large porous materials. For comparison, the wall thickness of MCM-41 type materials is usually in the range of 10–20 Å. Alumina by-products have not be found. EDX analysis revealed a homogeneous distribution of aluminum throughout the samples. Scanning electron micrographs of selected samples show that the ordered structured materials may crystallize as in well shaped particles. In has been reported that the morphology of ordered mesoporous molecular sieves depend strongly on the synthesis conditions [10]. Al-MMS-100 crystallized in form of intergrown disc-like particles with sizes of 5–10 μm (Fig. 3).

3.2. Characterization

Textural properties like pore size and distribution, specific surface areas and volume were determined by nitrogen

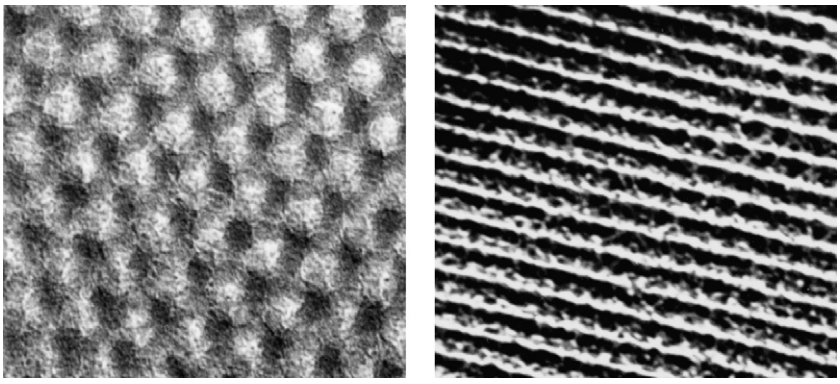

Fig. 2. TEM images of nanoporous aluminosilicate having pore size ca. 100 Å along (left) and perpendicular (right) to the pore direction.

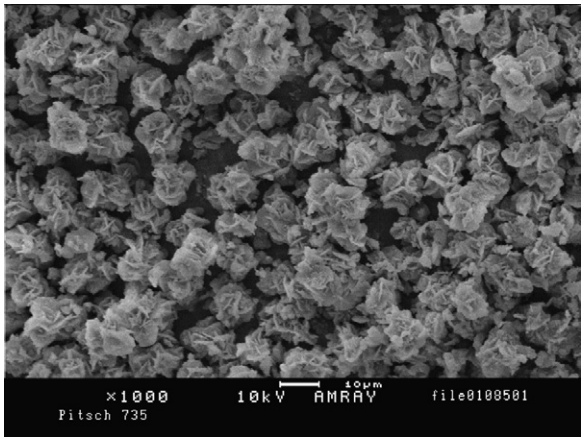

Fig. 3. SEM image of calcined Al-MMS.

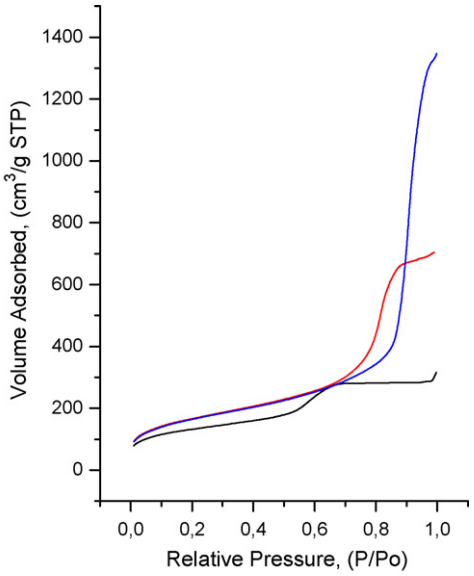

Fig. 4. Nitrogen adsorption isotherms of Al-MMS-50, Al-MMS-100 and Al-MMS-200 (from bottom to top).

adsorption–desorption measurements (Fig. 4). The sorption isotherms show the typical course observed with mesoporous materials. The first up-take at low a relative pressure p/p_0 is due to surface layer adsorption followed by multi layer adsorption. The second adsorption step in the isotherm is related to capillary condensation of nitrogen in the meso- or nano-pores. The small hysteresis in the adsorption–desorption curve point to large pore openings and free accessibility of the internal pore volume. The pore size maxima of considered Al-MMS samples are ca. 50, 100 and 200 Å, respectively. The width of pore size distribution increases with growing pore size (Fig. 5). The specific pore volumes range from ca. 0.5 to 2 cm^3/g and depend strongly on the synthesis conditions like temperature, thermal pre-altering, crystallization temperature and time as well as on the chemical compositions. Using this method, mesoporous materials with Si/Al ratios down to 1.4 could be prepared. With growing Si/Al ratio, the specific surface areas and pore volume increase (Table 1). This is inline with earlier findings with MCM-41 tape materials. It might be that the aluminum influences network formation due by restriction the flexibility of T–O–T bridging angles between the AlO_4 and SiO_4 tetrahedra. The synthesis conditions for considered different pore sized Al-MMS-50, Al-MMS-100 and Al-MMS-200 are given in Table 2.

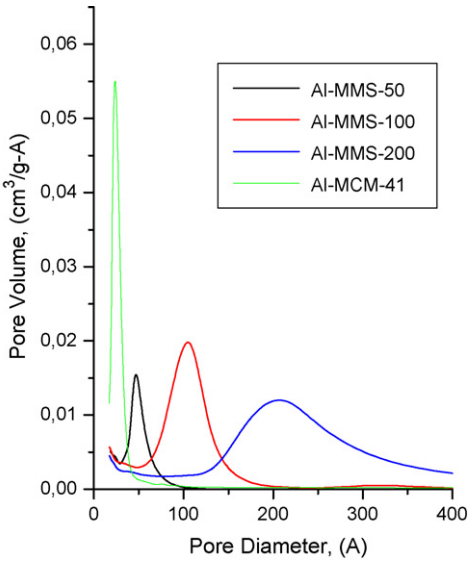

Fig. 5. Pore size distributions derived from nitrogen sorption measurements of Al-MCM-41, Al-MMS-50, Al-MMS-100 and Al-MMS-200 (from left to right).

In the ^{27}Al MAS solid state NMR spectra of as-synthesized Al-MMS samples appear two main signals at ca. 60 ppm and near 0 ppm. They correspond to tetrahedral coordinated framework Al^{IV} and extra-framework octahedral coordinated Al^{VI} units (Fig. 6). After calcinations, the Al^{IV} content decreases. Simultaneously, a signal for fivefold coordinated Al^{V} appears. Interestingly, treat-

Table 1
Influence of the crystallization conditions on the specific surface area and pore volume proper of AL-MMS materials.

Sample	Si/Al ratio gel	Si/Al ratio material	Crystallization conditions	Surface area BET [m^2/g]	Pore volume BJH [cm^3/g]
Al-MMS-50	11.3	12.3	1 d/60 °C	473	0.42
Al-MMS-100	11.1	13.3	20 h/35 °C;4 d/100 °C	595	1.01
Al-MMS-200	11.2	12.1	20 h/35 °C;4 d/100 °C organic additive	588	2.01

Table 2
Influence of of the Si/Al ratio in the synthesis gel on the concentration of cation sites, i.e. potential Brønsted sites and textural propoerties.

Si/Al ratio gel	Si/Al ratio material	NH_4^+ exchange capacity [mmol/g]	BET surface area [m^2/g]	Specific pore volume [cm^3/g]
1.0	1.4	0.10	317	0.19
4.6	5.8	0.39	505	1.12
7.3	9.8	0.33	627	1.09
10.7	1.5	0.39	602	0.95
17.7	21.9	0.32	900	1.41
∞	∞	0.0	820	1.10

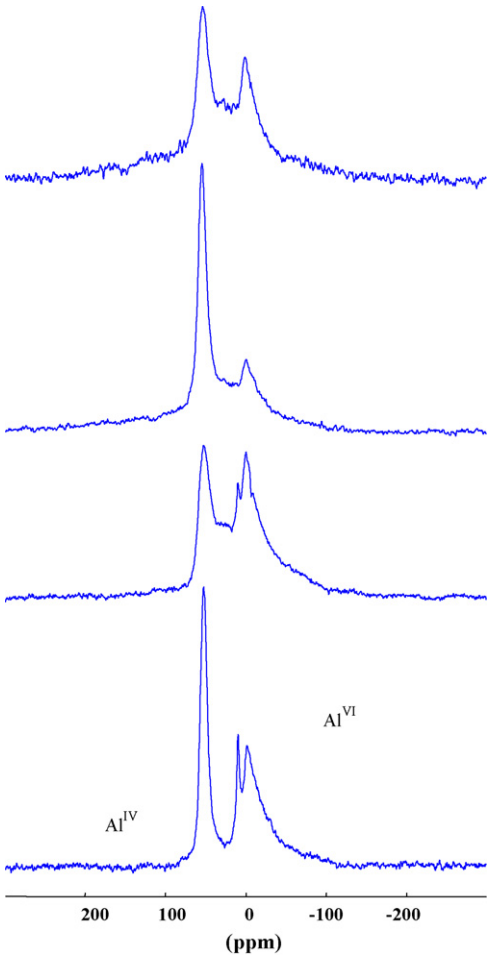

Fig. 6. ^{27}Al MAS NMR spectra of Al-MMS-100 after different steps of activation. From bottom to top: as-synthesized and dried at 70 °C, calcined at 550C, NH_4-exchanged, and the calcined NH_4-form.

ment in diluted aqueous ammonium nitrate solution leads to a markedly increase of the intensity of the Al^{IV} signal, usually related to Brønsted acid sites. It is now dominating. The intensity changes are not due to dissolution of extra-framework Al^{VI} species. Calcination of the ammonium exchanged molecular sieve to get the Brønsted acidic H-form leads again to a decrease of Al^{IV} and increase of Al^{VI} and Al^{V} species. However, the relative amount of Al^{IV} units is improved in comparison to the material obtained after the first calcinations. After contacting with moisture or water treatment again the Al^{IV} signal is dominating. Hence, the framework is very flexible and undergoes structural re-arrangements during different treatments. Therefore, differences in sample pretreatments may also contribute to the observation of different Al^{IV} to Al^{VI} ratios for similar mesoporous materials reported in the literature [16,20,21]. However, Al-rich materials (Si/Al–1.4) contain penta- and octahedral coordinated aluminum beside tetrahedral Al species.

Structural re-arrangements during the activation procedure are evidenced by solid state ^{29}Si MAS NMR spectra especially for Al-MMS with Si/Al = 21.9 (Fig. 7). The spectrum of the as-synthesized material is well structured showing three overlapping lines corresponding to twofold, threefold and fourfold connected SiO_4-tetrahedron centered at ca. −92, −102 and 107 ppm, also denoted as Q^2, Q^3 and Q^4 silicon sites, respectively [28,29]. After calcination, signal lines are broadened and not resolved. Obviously, condensation of SiO_4-tetrahedron and corresponding formation of Si–O–Si brides increases the width of the Si–O–Si bridging angle distribution. After aqueous ammonium exchange the network relaxes or partially hydrolysis resulting again in more resolved ^{29}Si NMR lines. However, the relative intensity, and hence concentration, of fourfold connected SiO_4-tetrahedron is increased. The lattice connectivity and stability is enhanced. Increasing Al-content results in broadened spectra and an overall low field shift. The low filed shift is mainly due to the substitution of Silicon by aluminum in tetrahedral network sites. The number of Si(1Al), Si(2Al) and Si(3Al) units increases. A clear discrimination between bond angle, connectivity and substitution effects on the chemical shifts and

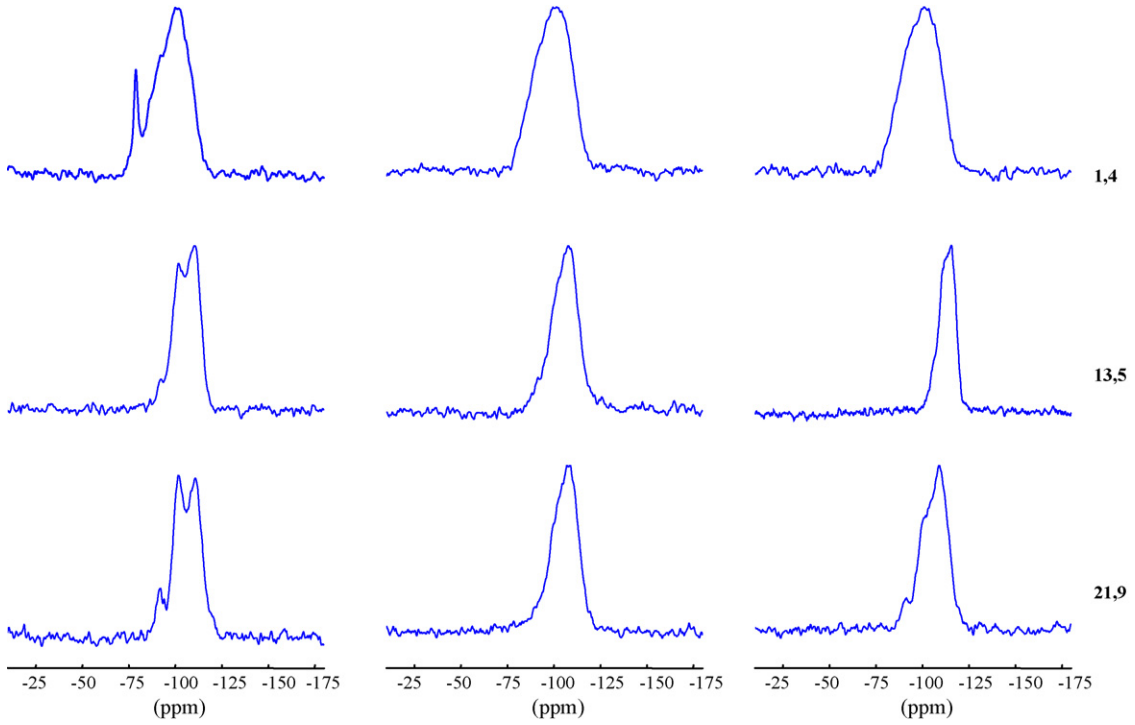

Fig. 7. ^{29}Si MAS NMR spectra of Al-MMS of with different Si/Al ratio (from left to right: dried as-synthesized, calcined at 550 °C and re-hydrated).

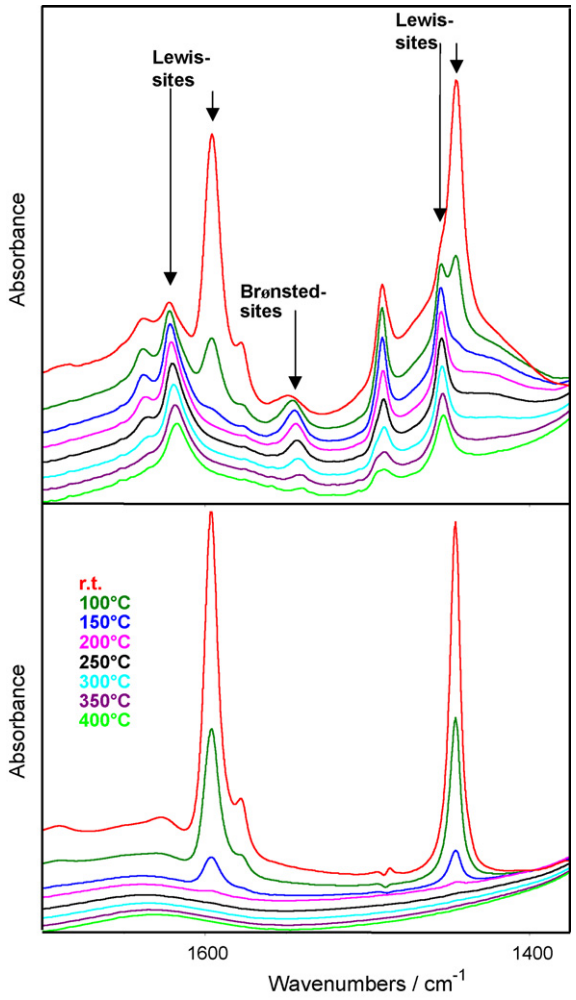

Fig. 8. Temperature-programmed FTIR spectra of pyridine desorption from H, Al-MMS-100 (above) and (below) Si-MMS (top—pyridine adsorbed at room temperature; thereafter, from top to bottom, starting desorption of pyridine 100 °C and to 400 °C in steps of 50 K).

appearance of the ^{29}Si NMR spectra requires more sophisticated investigations.

FTIR spectra of adsorbed pyridine the presence of Brønsted (BS) and Lewis sites (LS) indicated by the absorbance at 1548 and 1445 cm^{-1}, respectively (Fig. 8). The concentration of both the types of sites increases with growing Al content. Some BS are strong. Even at 400 °C some intensity of the 1548 cm^{-1} absorbance related BS sites remains in the spectrum. In contrast, pure Si-MMS is not acidic. Neither a BS band nor strong LS giving rise to absorbance at 1445 and ca. 1630 cm^{-1} are observed. Coordinative bound pyridine is desorbed below 200 °C.

The acidity of Al-MMS samples was additionally investigated by temperature-programmed ammonia desorption experiments—NH_3-TPD (Fig. 9). To distinguish between LS and BS bound ammonia, ammonia loaded H, Al-MMS as well as NH_4^+ exchanged Al-MMS were studied. Ammonia loaded samples show

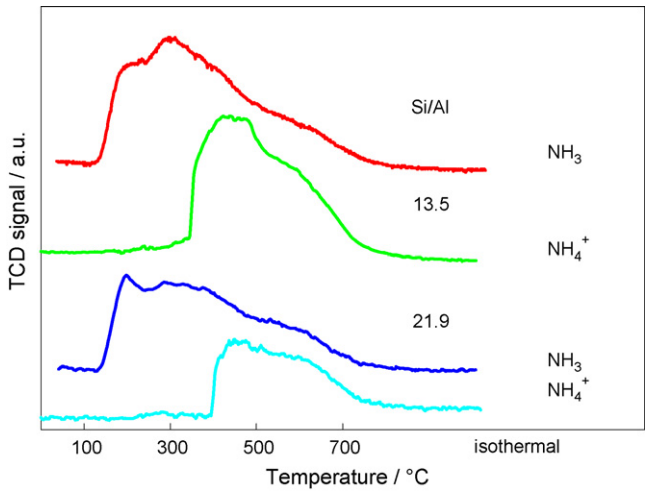

Fig. 9. Comparison of NH_3-TPD curves of ammonia loaded and ammonium exchanged Al-MMS-100: with Si/Al = 13.5 and Si/Al = 21.9.

higher site concentration especially at low temperature between 120 and 300 °C. Desorption of ammonia from NH_4^+ exchanged Al-MMS start at 350 °C for AL-MMS (Si/Al = 13.5). The desorption temperature increases with growing Si/Al ratio to ca. 400 °C for Al-MMS (Si/Al = 21.9). Hence, it can be concluded, that the Si/Al ratio has a great influence on the acidic strength of BS even in large mesoporous networks with amorphous wall structures. The acid strength of sites is relatively strong as indicated by high desorption temperature of ammonia from ammonium exchanged samples starting at 350–400 °C in the NH_3-TPD spectra. The high-temperature desorption branch above 500 °C is most likely due to desorption of re-adsorbed ammonia from strong Lewis sites.

The chemical stability of Al-MMS materials was investigated by treatment of calcined and silylated samples in propanol, water and sodium carbonate solution (pH = 11.4) at 60 °C. temperature. Textural changes were studied by nitrogen sorption measurements. For comparison, a Si-SBA-15 was included. After treatment in alkaline solution, a 30% loss in specific surface area was found with Si-SBA-15. In contrast, the Al-substituted MMS samples showed only minor loss by ca. 5%. This result shows the advanced stability of Al containing MMS. Organosilylation stabilizes generally the materials. However, a loss of grafted silanes of 10–20% based on N-analysis was observed for both types of materials after treatment in sodium carbonate solution.

3.3. Catalysis

3.3.1. Acid catalysis

The catalytic performance of Al-MMS samples was tested in the benzoylation of anisole with benzoic anhydride (Scheme 1).

This reaction is sensitive to Brønsted acid sites. The reactivity observed with Al-MMS samples confirms the Brønsted acidic character of acid sites. The conversion increases with Al-content of Al-MMS samples (Fig. 10). The Al-content is related to the concentration of Brønsted sites. This confirms conclusion derived from

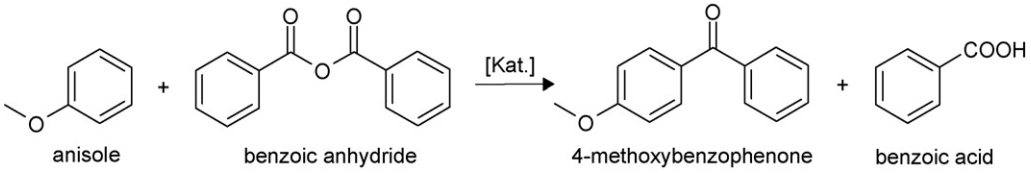

Scheme 1.

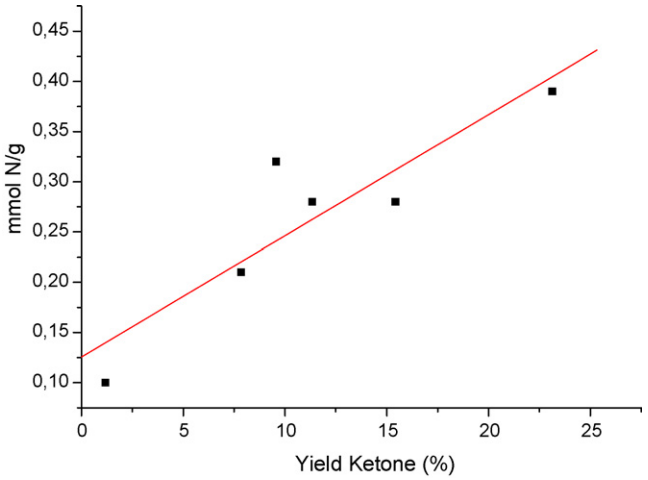

Fig. 10. Influence of the Brønsted site concentration in Al-MMS samples, expressed as ammonium ion exchange capacity N, on the catalytic activity (conversion). Test reaction: benzoylation of anisole with benzoic anhydride.

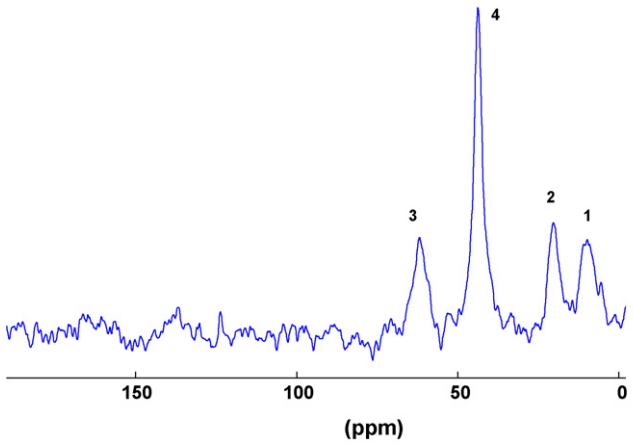

Fig. 11. ^{13}C MAS NMR spectrum of N-(dimethyl) aminopropyl grafted Al-MMS-100 (4- signal of methyl group C-atoms, signal 1, 2 and 3 belonging to the different C-atoms of the propyl group).

^{27}Al NMR spectra and FTIR and TPD experiments. The Maximum conversion of ca. 23% was reached Al-MMS sample with Si/Al = 5.8. Deviations from the straight line in Fig. 10 are probably due to pore blockages. Indeed, propylsulfonic grafted Al-MMS with high loadings (up to 1.3 mmol/g) were surprisingly not catalytic active. Obviously, starting materials are adsorbed at acid sites at the low temperature of reaction. Thereby mobility is restricted in the confined space of the pores. Elemental analysis showed enhanced C:S ratios for all sulfonic acid functionalized samples. The grafting of propylsulfonic acid functions was proven by ^{13}C MAS NMR spectroscopy. Due to partial pore filling, the specific pore volume and pore diameter were decreased.

3.3.2. Base catalysis

Base catalysts were obtained by grafting of aminopropyl and N-(dimathyl) aminopropyl functions. The grafting was controlled by CHN analysis of samples, nitrogen sorption experiments (Fig. 11) and ^{13}C MAS NMR spectrometry (Fig. 12). All confirm the grafting by nitrogen and carbon content and C:N ratio, decreased pore volume and size as well by the appearance of the corresponding ^{13}C NMR limes and line intensity ratios of carbon nuclei at different positions in the propylsilyl group.

The catalytic activity of the base functionalized amino alkylamino grafted MMS was studied in the Michael addition of methyl-vinyl-ketone and 2-methyl-cyclohexane-1,3-dione to the bulky 2-(γ-oxybutyl)-2-methyl-cyclohexan-1,3-dione (Scheme 2).

The conversions over mesoporous catalysts of different pore size are shown are shown in Fig. 13. Basic functionalized A-MMS 50 and Al-MMS-100 catalysts were used. For comparison, also a small porous MCM-48 catalyst was tested. The on-set conversion is highest with aminopropyl silyted MMS-100 and MCM-48 samples (top curve in Fig. 13), whereas N-(dimethyl) aminopropyl modified MCM-48 (middle curve) and Al-MMS (bottom curve) are less active. Possibly, the secondary amine sites are less accessible in the confined space of nanopores. The high activity of functionalized MCM-48, which has a pore size of ca. 30 Å, tends to show the importance of the pore connectivity besides the pore size. MCM-48contains a pseudo three-dimensional pore system which Y-shaped pore intersections providing concave and convex pore surfaces. All catalysts work highly selective (97%). Nearly complete conversion was achieved after 20 h.

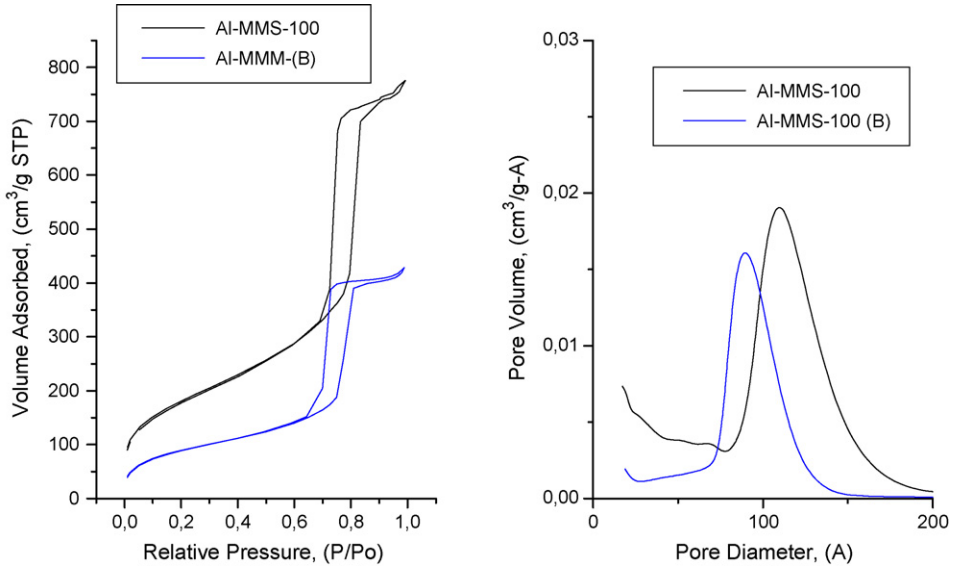

Fig. 12. Decrease of nitrogen adsorption capacity and pore size caused by grafting of aminopropyl functions in the pores of Al-MMS-100 B compared to the unloaded sample, Nitrogen sorption isotherms (left), pore size distribution (right).

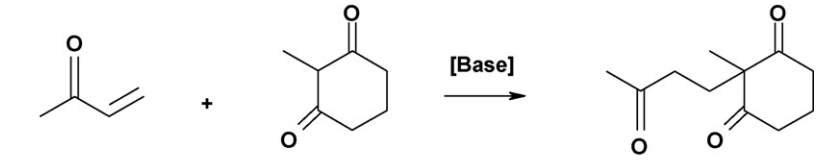

Methylvinylketon 2-Methyl-cyclohexan -1,3-dion 2-Methyl-cyclohexan -1,3-dion

Scheme 2.

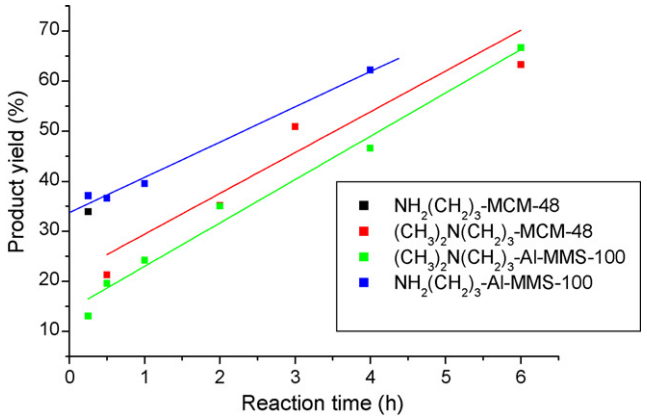

Fig. 13. Comparison of the catalytic activity of nanoporous and mesoporous catalysts (MMS and MCM-48) functionalized with primary and secondary amine in the Michael addition of methyl-vinyl-ketone and 2-methyl-cyclohexane-1,3-dione.

4. Conclusion

The use of reactive inorganic silica and alumina precursors in the template assisted synthesis of nanoporous materials allows the preparation of novel large porous Al-substituted materials with highly ordered pores of uniform size. They are especially characterized by large specific surface areas and pore volumes, high aluminum content with Si/Al ratios ranging from 5 to 25, thick pore walls of 40–50 Å, medium strong to strong Brønsted sites besides Lewis acidity, and improved stability against alkaline solution. The internal pores are ell accessible for molecules allowing the use as catalyst support or catalyst even for the conversion or formation of large molecules.

Acknowledgement

The authors thank Drs. M. Schneider and U. Bentrup for kind providing X-ray difraction and FTIR measurements.

References

[1] A. Wan, Y. Shi, D. Zhao, Chem. Commun. (2007) 897.
[2] B. Onida, S. Fiorilli, B. Camarota, D. Perrachon, M.C. Bruzzzoniti, Stud. Surf. Sci. Catal. Series 174 (2008) 67.
[3] B. Onida, L. Borello, C. Busco, P. Ugliengo, Y. Goto, S. Inagaki, E. Garrone, J. Phys. Chem. B 109 (2005) 11961.
[4] R. Nicolas, F. Berube, T.W. Kim, M. Thommes, F. Kleitz, Stud. Surf. Sci. Catal. Series 174 (2008) 41.
[5] J.S. Beck, J.C. Vartuli, G.J. Kennedy, C.T. Kresge, W.J. Roth, S.E. Schramm, Chem. Mater. 6 (1994) 1816.
[6] O.C. Gobin, Y. Wang, D. Zhao, F. Kleitz, S. Kaliaguine, J. Phys. Chem. C 11 (2007) 3053.
[7] M. Miyahara, A. Vinu, K. Ariga, J. Nanosci. Nanotechnol. 6 (2006) 1765.
[8] M. Kruk, M. Jaroniec, C.H. Ko, R. Ryoo, Chem. Mater. 12 (2000) 1961.
[9] A. Vinu, V. Murugesan, W. Böhlmann, M. Hartmann, J. Phys. Chem. B 108 (2004) 11496.
[10] W. Li, S.B. Liu, M.O. Coppens, Langmuir 21 (2005) 2078.
[11] T.W. Kim, F. Kleitz, B. Paul, R. Ryoo, J. Am. Chem. Soc. 127 (2005) 7601.
[12] H. Cai, D.Y. Zhao, Sci. China Ser. B Chem. 52 (2009) 1090.
[13] X. Zhang, F. Zhang, X. Yan, Z. Zhang, F. Sun, Z. Wang, D. Zhao, J. Porous Mater. 15 (2008) 145.
[14] B. Xu, W. Hua, Y. Yue, Y. Tang, Z. Gao, Catal. Lett. 100 (2005) 95.
[15] F. Zhang, Y. Yan, H. Yang, Y. Mng, C. Yu, B. Tu, D. Zhao, J. Phys. Chem. B 109 (2005) 8723.
[16] Z. Luan, M. Hartmann, D. Zhao, W. Zhou, L. Kevan, Chem. Mater. 11 (1999) 1621.
[17] T. Klimova, J. Reyes, O. Gutierrez, L. Lizama, Appl. Catal. A: Gen. 335 (2008) 159.
[18] M. Cheng, Z. Wang, K. Sakurai, F. Kumata, T. Saito, T. Komatsu, T. Yashima, Chem. Lett. 28 (1999) 131.
[19] M. Gomez-Cazalilla, J.M. Merida-Robles, A. Gurbani, E. Rodriguez-Castellon, A. Jimenez-Lopez, Solid State Chem. 180 (2007) 1130.
[20] X. Liang, J. Li, Q. Lin, K. Sun, Catal. Commun. 8 (2007) 1901.
[21] W. Hu, Q. Luo, Y. Su, L. Chen, Y. Yue, C. Ye, F. Deng, Micropor. Mesopor. Mater. 92 (2006) 22.
[22] O.A. Anunziata, A.R. Beltramone, M.L. Martiniz ans, L.L. Belon, J. Colloid Interface Sci. 315 (2007) 184.
[23] V. Dufand, M.E. Davis, J. Am. Chem. Soc. 125 (2003) 9403.
[24] X. Wang, K.S. Lin, J.C. Chan, S. Chen, J. Phys. Chem. B 109 (2005) 1763.
[25] J.M. Kim, S.-E. Park, G.D. Stucky, Stud. Surf. Sci. Catal. Series 135 (2001) 286.
[26] H. Kosslick, G. Lischke, B. Parlitz, W. Storek, R. Fricke, Appl. Catal. A: Gen. 184 (1999) 49.
[27] H. Kosslick, G. Lischke, H. Landmesser, B. Parlitz, W. Storek, R. Fricke, J. Catal. 176 (1998) 102.
[28] A.D. Irwin, J.S. Holmgren, J. Jonas, J. Mater. Sci. 23 (1988) 2908.
[29] G. Engelhardt, D. Michel, High Resolution Solid State NMR of Silicates and Zeolites, Wiley, Chichester, 1987.